

Characterization of Ca^{2+} -activated Cl^- currents in mouse kidney inner medullary collecting duct cells

Zhiqiang Qu, Raymond W. Wei, and H. Criss Hartzell

Department of Cell Biology, Emory University School of Medicine, Atlanta, Georgia 30322-3030

Submitted 23 January 2003; accepted in final form 24 April 2003

Qu, Zhiqiang, Raymond W. Wei, and H. Criss Hartzell. Characterization of Ca^{2+} -activated Cl^- currents in mouse kidney inner medullary collecting duct cells. *Am J Physiol Renal Physiol* 285: F326–F335, 2003. First published April 29, 2003; 10.1152/ajprenal.00034.2003.— Ca^{2+} -activated Cl^- (ClCa) channels were characterized biophysically and pharmacologically in a mouse kidney inner medullary collecting duct cell line, IMCD-K2. Whole cell recording was performed with symmetrical *N*-methyl-D-glucamine chloride (NMDG)-Cl in the intracellular and extracellular solutions, and the intracellular Ca^{2+} concentration ($[\text{Ca}^{2+}]_i$) was adjusted with Ca^{2+} -EGTA buffers. The amplitude of the current was dependent on $[\text{Ca}^{2+}]_i$. $[\text{Ca}^{2+}]_i < 800$ nM strongly activated outwardly rectifying Cl^- currents, whereas high Ca^{2+} (21 μM) elicited time-independent currents that did not rectify. The currents activated at low $[\text{Ca}^{2+}]_i$ exhibited time-dependent activation and deactivation. The affinity of the channel for Ca^{2+} was voltage dependent. The EC_{50} for Ca^{2+} was ~ 0.4 μM at +100 mV and ~ 1.0 μM at -100 mV. The Cl^- channel blocker niflumic acid in the bath equally inhibited both inward and outward currents reversibly, with a $K_i = 7.6$ μM . DIDS, diphenylamine-2-carboxylic acid, and anthracene-9-carboxylic acid reversibly inhibited outward currents in a voltage-dependent manner. DTT slowly inhibited the currents, but tamoxifen did not. Comparing the biophysical and pharmacological properties, we conclude that IMCD-K2 cells express the same type of ClCa channels as those we have described in detail in *Xenopus laevis* oocytes (Qu Z and Hartzell HC. *J Biol Chem* 276: 18423–18429, 2001).

patch clamp; calcium; chloride channel; biophysics; pharmacology

Ca^{2+} -ACTIVATED Cl^- (ClCa) channels perform important physiological functions, including epithelial secretion, repolarization of cardiac action potential, regulation of vascular tone, olfactory transduction, neuronal excitability, and fast block to polyspermy (2, 9, 13, 23, 26, 30, 33).

The kidney plays a critical role in salt secretion and absorption, and Cl^- channels are an important component of this process. Determining the roles of different types of Cl^- channels is an area of active investigation. The inner medullary collecting duct (IMCD) is the final segment of the kidney involved in determining acid-base balance and urinary salt composition. In the IMCD, both electrogenic Na^+ absorption and electro-

genic Cl^- secretion participate in the regulation of overall NaCl balance (41, 42). Na^+ reabsorption in the IMCD occurs predominantly via apical amiloride-sensitive Na^+ channels and a basolateral $\text{Na}^+\text{-K}^+\text{-ATPase}$. The activities of other transporters such as $\text{Na}^+\text{-K}^+\text{-2Cl}^-$ and $\text{Na}^+\text{-Cl}^-$ cotransporters and the Na^+/H^+ exchanger may also be involved in Na^+ homeostasis (50). The IMCD also has the capacity to secrete anions. The CFTR (21, 48), ClCa channels, swelling-activated Cl^- currents (3, 4, 45), and ClC channels (24) have been implicated in the process. Na^+ absorption and Cl^- secretion in the IMCD are controlled by a wide variety of hormones and renal autacoids (20, 22, 41, 42, 50). For instance, mineralocorticoids augment the activities of both apical Na^+ channels and basolateral $\text{Na-K}^+\text{-ATPase}$, whereas atrial natriuretic peptides bind to guanylate cyclase-linked receptors, leading to inhibition of apical Na^+ channel function (50). Anion secretion can be affected by changes in intracellular cAMP or Ca^{2+} (4, 21).

The purpose of this study was to characterize in detail the ClCa currents in IMCD-K2 cells. IMCD-K2 cells were established from the initial portion of the IMCD of a mouse transgenic for SV40 (27). The cell line retains features typical of IMCD: cyclic nucleotide-gated cation channels in the apical membrane mediate mineralocorticoid-sensitive Na^+ absorption that is inhibited by amiloride (27). Moreover, this cell line exhibits electrogenic Cl^- secretion (27). A recent study presented evidence that mouse IMCD-K2 cells possess two separate apical Cl^- conductances that are activated by intracellular cAMP or Ca^{2+} , respectively (3). ClCa currents in IMCD-K2 cells showed voltage-dependent kinetic changes in whole cell recording. After the induction of slow ramps in $[\text{Ca}^{2+}]_i$ produced by exposing BAPTA-loaded IMCD-K2 cells to ionomycin, whole cell currents exhibited pronounced outward rectification with time dependence. ClCa currents in another IMCD cell line, IMCD-K3, exhibited somewhat different properties (40) (see DISCUSSION).

Our laboratory has studied ClCa channels in *Xenopus laevis* oocytes extensively (18, 28, 29, 31, 32, 38, 39). ClCa channels in oocytes resemble Ca^{2+} -activated Cl^- channels expressed in some mammalian cells such as parotid acinar cells, lacrimal gland cells, and pan-

Address for reprint requests and other correspondence: Z. Qu, Dept. of Cell Biology, 535 Whitehead Bldg., Emory Univ. School of Medicine, 615 Michael St., Atlanta, GA 30322-3030 (E-mail: zuq@cellbio.emory.edu).

The costs of publication of this article were defrayed in part by the payment of page charges. The article must therefore be hereby marked "advertisement" in accordance with 18 U.S.C. Section 1734 solely to indicate this fact.

creatic acinar cells (33). They are activated directly by intracellular Ca^{2+} , with a K_d in the $1\ \mu\text{M}$ range, exhibit different voltage-dependent kinetics at low and high Ca^{2+} concentrations ($[\text{Ca}^{2+}]_i$) and possess an anion selectivity sequence of $\text{I} > \text{Br} > \text{Cl}$. However, ClCa channels in other cells are different (33). Ca^{2+} activation of ClCa currents in colonic T84 and Jurkat T cells is mediated by Ca^{2+} /calmodulin-regulated protein kinase II, whereas ClCa currents in olfactory receptors have a low Ca^{2+} affinity, with a K_d of $26\ \mu\text{M}$ and an anion selectivity sequence of $\text{Cl} > \text{F} > \text{I} > \text{Br}$. Therefore, it seems that different types of ClCa channels exist in different cell types. We have described the "signature properties" of the *X. laevis* oocyte-type of ClCa channels (see Table 1 in Ref. 33). Stated simply, Ca^{2+} directly activates the channel without phosphorylation. The channel has a voltage-dependent Ca^{2+} affinity (in the $1\ \mu\text{M}$ range) such that, at a $[\text{Ca}^{2+}]_i$ of $< 1\ \mu\text{M}$, the currents strongly outwardly rectify and are time dependent. However, at high $[\text{Ca}^{2+}]_i$, the currents show a linear current-voltage (*I-V*) relationship and are time independent. The channel is more permeant to larger halide anions than to smaller ones ($\text{I} > \text{Br} > \text{Cl}$). The Cl channel blockers anthracene-9-carboxylic acid (A9C), diphenylamine-2-carboxylic acid (DPC), and DIDS block the channel from the outside in a voltage-dependent manner.

In this study, we applied whole cell recording to IMCD-K2 cells and observed Ca^{2+} activation by directly changing $[\text{Ca}^{2+}]_i$. Lower Ca^{2+} ($< 800\ \text{nM}$) activated outwardly rectifying Cl^- currents, whereas high $[\text{Ca}^{2+}]_i$ elicited nearly linear Cl^- currents. The currents activated at low $[\text{Ca}^{2+}]_i$ were time dependent for activation and deactivation. The Ca^{2+} activation and the Ca^{2+} affinity of the channel were voltage dependent. The Cl^- channel blocker niflumic acid (NFA) in the bath equally inhibited both inward and outward currents reversibly, with a $K_i = 7.6\ \mu\text{M}$. DIDS, DPC, and A9C reversibly inhibited outward currents in a voltage-dependent manner. These biophysical and pharmacological characteristics are so similar to those in *X. laevis* oocytes that we conclude that the ClCa channels expressed in IMCD-K2 cells and in *X. laevis* oocytes are very similar.

METHODS

Cell Culture

Mouse kidney IMCD-K2 cells were kindly provided by Dr. Bruce A. Stanton (Dartmouth Medical School, Hanover, NH), routinely cultured (*passages 14–36*) in PC-1 medium (Bio-Whittaker, Walkersville, MD) supplemented with PC-1 supplement (Bio-Whittaker), 10% heat-inactivated fetal bovine serum (Hyclone, Logan, UT), 2 mM L-glutamine (Life Technologies, Grand Island, NY), 50 U/ml penicillin, and 50 $\mu\text{g}/\text{ml}$ streptomycin (Life Technologies) in tissue culture flasks (Costar, Cambridge, MA) coated with Vitrogen plating media containing DMEM (Life Technologies), human fibronectin (10 $\mu\text{g}/\text{ml}$, Collaborative Biomedical, Bedford, MA), 1% Vitrogen 100 (purified collagen; Cohesion, Palo Alto, CA), and BSA (fraction V, 10 $\mu\text{g}/\text{ml}$; Sigma, St. Louis, MO), and maintained in a 37°C and 5% CO_2 incubator. For experiments, cells were

seeded onto glass coverslips (Fisher Scientific, Pittsburgh, PA) and used 1–3 days later.

Whole Cell Patch-Clamp Recordings

Current recordings from mammalian cells were made using a whole cell configuration. Whole cell currents were recorded with borosilicate glass electrodes (Sutter Instrument), pulled by a Sutter P-2000 puller, and fire polished. Pipette resistances were 2–5 M Ω . Whole cell patch-clamp data were acquired with an Axopatch 200A amplifier controlled by a Clampex 8.1 via a Digidata 1322A analog-to-digital and digital-to-analog converter (Axon Instruments), sampled at 2 kHz, and filtered at 1 kHz with a four-pole low-pass Bessel filter. The bath was grounded via a 3 M KCl-agarose bridge connected to an Ag-AgCl reference electrode. Bath solution changes were performed with a group of sewer pipes, having an 100- μm internal diameter, connected to the gravity-fed solution containers so that the solution bathing the cells could be changed in $\sim 2\ \text{ml}/\text{min}$.

Solutions

Symmetrical Cl^- solutions containing $\sim 150\ \text{mM}$ Cl were usually used for the whole cell recordings. Pipette solutions contained (in mM) 150 *N*-methyl-D-glucamine chloride (NMDG)-Cl, 10 HEPES-NMDG (pH 7.3), and 10 EGTA-NMDG or 10 Ca^{2+} -EGTA-NMDG. The bath solution contained (in mM) 140 NMDG-Cl, 4.5 KCl, 1 MgCl_2 , 2 CaCl_2 , and 10 HEPES-NMDG (pH 7.4). Sucrose was used to adjust osmolarity. In some experiments, NMDG $^+$ was replaced with K^+ in the pipette solution and with Na^+ in the bath solution. Mg-ATP (2 mM; Sigma) was also added to the pipette solution.

To obtain submicromolar concentrations of free Ca^{2+} , we buffered solutions with EGTA using the method of Tsien and Pozzan (47). The stock solution of Ca^{2+} -EGTA was made by the pH-metric method (47). Working solutions having different free Ca^{2+} were prepared by mixing the 0Ca^{2+} -EGTA solution with the Ca^{2+} -EGTA solution (Molecular Probes) in various ratios. The free $[\text{Ca}^{2+}]$ was calculated from the equation $[\text{Ca}^{2+}] = K_d \times [\text{Ca}^{2+}\text{-EGTA}]/[\text{EGTA}]$, where K_d is the K_d of EGTA ($K_d = 1.0 \times 10^{-7}\ \text{M}$ at 24°C , pH 7.3, ionic strength 0.16 M). The calculated Ca^{2+} concentrations were confirmed in each solution by fura 2 (Molecular Probes) measurements using an LS-50B luminescence spectrophotometer (PerkinElmer, Norwalk CT).

Anion Channel Blockers

NFA, DPC, and tamoxifen were purchased from Sigma, A9C was from Aldrich Chemical, and DIDS was from Molecular Probes. DIDS was suspended in water at 0.3 M as a stock before working solutions were made. Other compounds were dissolved in DMSO at 0.3 M as stocks to keep the DMSO concentration in working solutions $< 0.1\%$. DL-DTT (Sigma) stock solution was made in H_2O .

Display and Analysis of Data

For the calculations and graphical presentation, we used Origin 6.0 software (Microcal). Curve fitting was performed using the iterative algorithms in Origin. Results are presented as means \pm SE, and *n* refers to the number of patches in each experiments. The significance of the difference between values was determined using Student's *t*-test (paired data) for tests between individual data pairs.

RESULTS

Activation of Cl^- Currents in Whole Cell Patches by Cytosolic Ca^{2+}

Figure 1 shows the biophysical characteristics of ClCa currents in an IMCD-K2 whole cell recordings. Both extracellular and cytosolic solutions contained NMDG-Cl, so that cation currents were minimized. The patches were held at -40 mV and stepped to a membrane potential (V_m) between -100 and $+100$ mV for 0.75 s and then stepped to -40 mV for 0.3 s. At <20 nM Ca^{2+} , only very small currents were recorded (Fig. 1A). However, when $[\text{Ca}^{2+}]$ was increased to 100 nM, a

slowly developing but sustained outward current was observed in response to depolarizing steps (Fig. 1B). Deactivating inward tail currents were observed on the return to -40 mV from depolarized potentials (Fig. 1B). Outward currents observed with 100 – 500 nM Ca^{2+} were composed of a small instantaneous time-independent component and a large slowly activating time-dependent component (Fig. 1, B–D). Very little steady-state inward current was observed at negative potentials at $[\text{Ca}^{2+}] < 500$ nM (Fig. 1, B and C). With $[\text{Ca}^{2+}] \geq 500$ nM, outward currents were increasingly dominated by the time-independent component and inward currents developed (Fig. 1, D and E). At $21 \mu\text{M}$

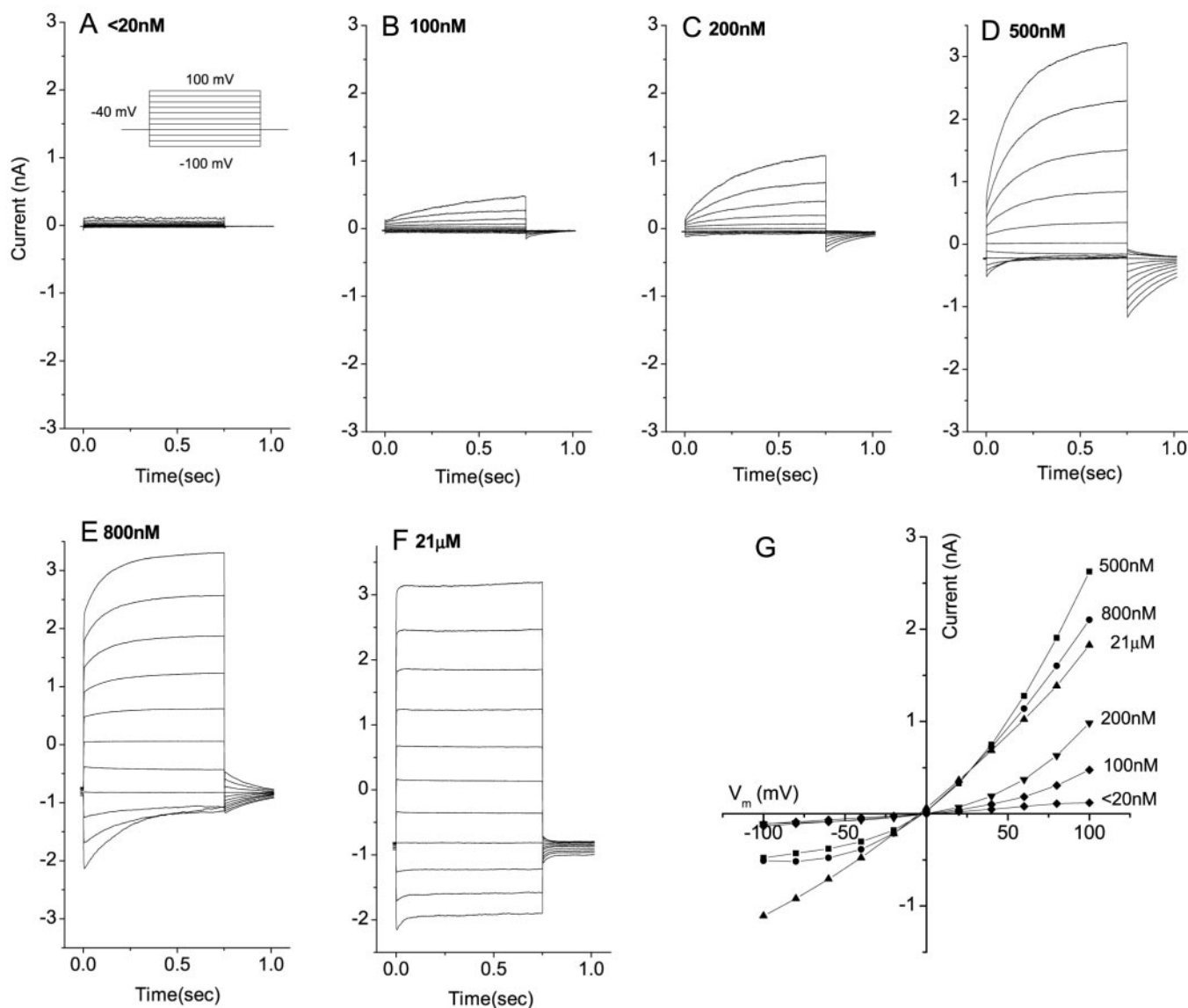


Fig. 1. Activation of Cl^- currents by intracellular Ca^{2+} in mouse IMCD-K2 cells. A–F: representative traces of Ca^{2+} -activated Cl^- currents recorded in whole cell configuration with various Ca^{2+} concentrations ($[\text{Ca}^{2+}]$) in pipette solutions. The whole cell patches were voltage clamped by stepping from a holding potential of -40 mV to various potentials between -100 and $+100$ mV for 0.75 s with a 20 -mV increment for each step, followed by a 0.3 -s step of -40 mV (voltage protocol is shown in *inset* in A). G: steady-state current-voltage (I - V) relationship for whole cell currents. The average currents at the end of the 0.75 -s pulse for different $[\text{Ca}^{2+}]$ were plotted vs. membrane potentials (V_m). Nos. of cells are 6, 10, 5, 5, 5, or 9, and SE are 31, 79, 69, 193, 317, 351 pA at 100 mV for <20 , 100, 200, 500, 800 nM, or $21 \mu\text{M}$ $[\text{Ca}^{2+}]$, respectively. Error bars are not shown for clarity.

Ca^{2+} , inward and outward currents were nearly equal in amplitude, and the currents became essentially instantaneous (Fig. 1F). Figure 1G shows that the steady-state I - V relationship changed from outwardly rectifying at <800 nM Ca^{2+} to almost linear at $21 \mu\text{M}$ $[\text{Ca}^{2+}]$. The currents reversed at Cl^- equilibrium potential. Note that the outward currents at 800 nM and $21 \mu\text{M}$ were smaller than that at 500 nM. We do not know whether this was caused by current rundown or whether the channel responded biphasically to Ca^{2+} . We prefer the explanation that Ca^{2+} has a biphasic effect. A similar phenomenon was observed in excised patches from *X. laevis* oocytes (28).

Similar experiments were done with 150 mM KCl on the intracellular side and 150 mM NaCl on the extracellular side. Similar results were obtained except that reversal potentials were shifted from ~ 0 with symmetrical NMDG (Fig. 1G) to about -10 mV with K^+/Na^+ (data not shown), indicating that nonselective cation

conductance may have contaminated the records under these conditions or that the channel is also slightly permeable for small cations.

Voltage-Dependent Ca^{2+} Affinity of ClCa Currents

The data in Fig. 1G indicate that the activation of ClCa currents is voltage dependent at a $[\text{Ca}^{2+}]$ between 100 and 800 nM. For further analysis, the voltage dependence of the ClCa currents at different $[\text{Ca}^{2+}]$ was determined by plotting conductance vs. V_m . Conductance was determined by measuring the instantaneous tail currents (see Fig. 1) at the beginning of the -40 -mV step after various voltage steps between $+100$ and -100 mV as shown in Fig. 1A and dividing by the driving force (-40 mV). Figure 2A shows the voltage dependence of the ClCa conductance at different $[\text{Ca}^{2+}]_i$. The average conductance-voltage curves ($n = 5$ – 12 different whole cell patches for each $[\text{Ca}^{2+}]$) show

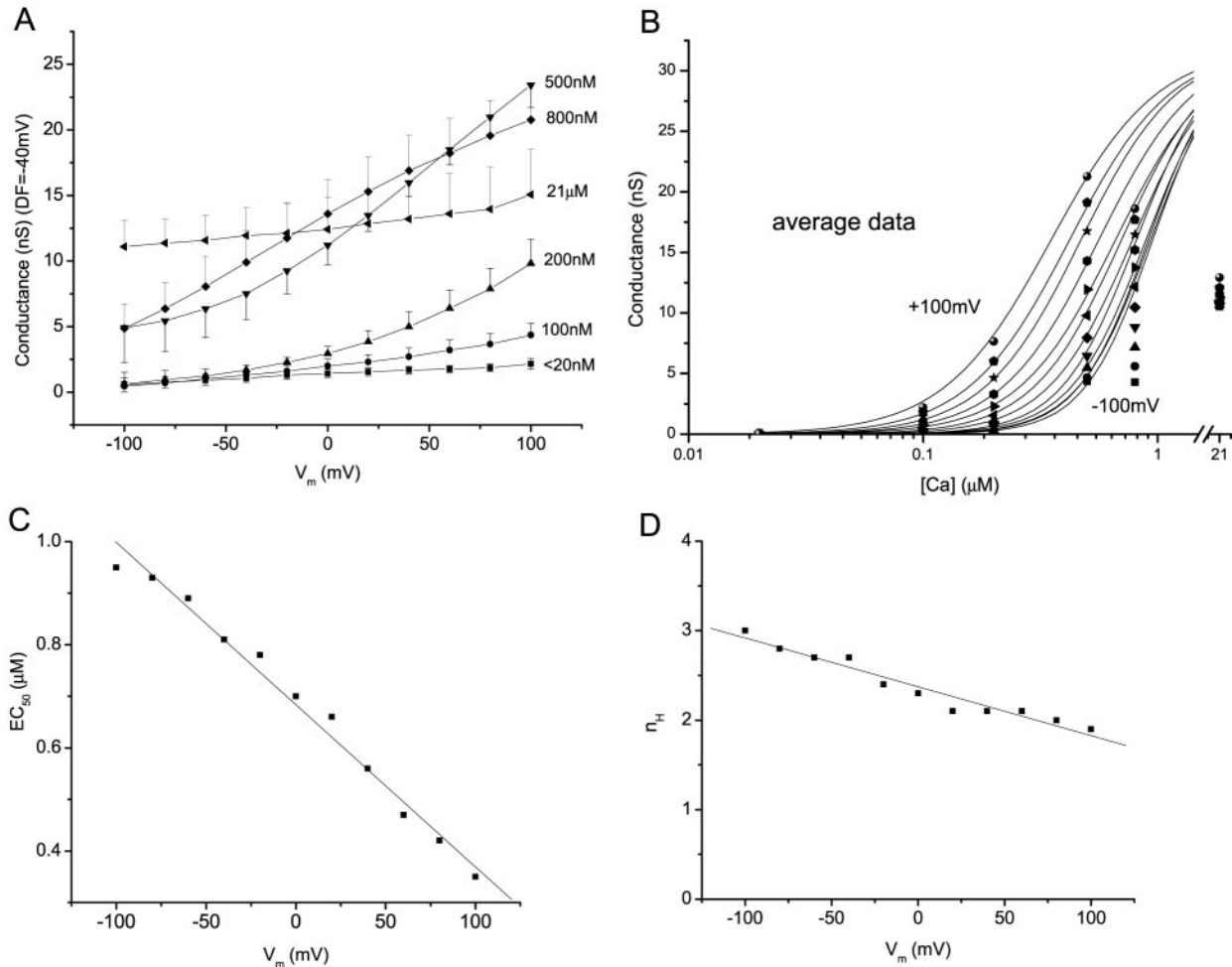


Fig. 2. Voltage-dependent Ca^{2+} affinity of Ca^{2+} -activated Cl^- (ClCa) currents in IMCD-K2 cells. **A**: voltage dependence of Ca^{2+} -dependent conductance of whole cell ClCa currents. Average conductance at various $[\text{Ca}^{2+}]$ was calculated by dividing the tail currents at the beginning of 0.3-s steps (shown in A–F in Fig. 1) by the driving force (-40 mV). **B**: average apparent affinity of the channel for Ca^{2+} at different voltages. The conductance in **A** was replotted as a function of $[\text{Ca}^{2+}]$. The data for <20 – 500 nM Ca were fitted to the Hill equation. Each curve represents a 20-mV increment. \bullet , $+100$ mV; \blacksquare , -100 mV. **C** and **D**: best-fit parameters of the data in **B** to the Hill equation. n_H , Hill coefficient; EC_{50} , apparent affinity of the channel for Ca^{2+} .

that increasing $[\text{Ca}^{2+}]$ from 100 to 500 nM shifted the conductance-voltage relationship strongly in the leftward direction and significantly increased the voltage dependence (increased the slope), indicating that the activation of the channel by Ca^{2+} is affected by V_m . We have previously shown that the effect of V_m on the Ca^{2+} activation of *X. laevis* oocyte ClCa channels is due to the voltage dependence of the channel for Ca^{2+} affinity.

To quantify the voltage dependence of the Ca^{2+} affinity of the channel, we plotted the mean conductance vs. $[\text{Ca}^{2+}]$ for each voltage (Fig. 2B). Only the data between <20 and 500 nM Ca^{2+} were fitted to the Hill equation. Data for 800 nM and 21 μM Ca^{2+} were not included when the average data were fitted to the Hill equation, because of the rundown of the current at these Ca^{2+} concentrations. The analysis shows that the apparent affinity of the channel for Ca^{2+} (EC_{50}) increased about threefold from 950 nM at -100 mV to 350 nM at $+100$ mV (Fig. 2C). The Hill coefficient ranged from 2 to 3 from -100 to $+100$ mV, indicating that more than one Ca^{2+} ion bound to the channel to activate it.

To fit the data to the Hill equation, we calculated a predicted maximum conductance (G_{max}) by fitting the conductance data for $+100$ mV and allowing all the parameters to float. We then assumed that this predicted G_{max} was the same for all voltages. The data for all voltages were then fit by fixing the G_{max} to this predicted G_{max} value. This approach assumes that the predicted G_{max} at 21 μM Ca^{2+} is larger than what is actually recorded. The recorded currents are smaller because of rundown or some secondary process. Using this method, the EC_{50} is estimated to be 350 nM at 100 mV and 950 nM at -100 mV. As an alternative method for estimating EC_{50} values, we measured the $[\text{Ca}^{2+}]$ that produced 50% of the observed conductance at 21 μM Ca^{2+} . This concentration was 169 nM at $+100$ mV and 550 nM at -100 mV. Therefore, although the EC_{50} values calculated by these two methods differ by about twofold, the conclusion is the same: the EC_{50} for Ca^{2+} is smaller at positive potentials than it is at negative potentials.

Pharmacological Properties of ClCa Currents in IMCD-K2 Cells

NFA. Figure 3 shows the block of ClCa currents by NFA applied to whole cell patched IMCD-K2 cells in the bath. NFA is one of the most commonly used Cl^- channel inhibitors. Cells were patched in the whole cell configuration with symmetrical NMDG- Cl^- solutions applied to intra- and extracellular sides and perfused with bath solutions containing different NFA concentrations. To observe the inhibition of inward and outward currents by blockers, a high- Ca^{2+} (21 μM Ca^{2+}) pipette solution was used to fully activate inward and outward currents.

Figure 3A shows *I-V* relationships recorded in the absence and presence of various concentrations of NFA in the bath. The whole cell patch was voltage clamped

from the holding potential of -40 mV with a 200-ms-duration voltage ramp from -100 to $+100$ mV. Inward and outward currents were almost equally blocked in a concentration-dependent manner. The current traces did not show a significant voltage-dependent block. In Fig. 3B, the averaged currents inhibited by each NFA concentration at $+100$ mV were expressed as a fraction of the current at $+100$ mV in the absence of NFA ($I/I_{\text{NFA}=0}$) and plotted as a function of NFA concentration. The data were fitted to the equation of the form

$$I/I_{\text{NFA}=0} = I_{\text{min}} + (I_{\text{max}} - I_{\text{min}})/(1 + ([\text{NFA}]/K_i)^n)$$

where I_{max} and I_{min} are the maximum and minimum current amplitudes, respectively, K_i is the concentration of NFA required to reduce the current amplitude to $(I_{\text{max}} + I_{\text{min}})/2$, and n is the slope factor. K_i at $+100$ mV for NFA is to 7.6 μM , with $n = 1.03$. Inhibition at 300 μM NFA is 93% for outward currents at $+100$ mV. Figure 3C shows that the averaged inhibition by 100 μM NFA is reversible. NFA was the most potent blocker we tested.

DIDS, DPC, and A9C. Three other Cl^- channel blockers, namely, DIDS, DPC, and A9C, exhibited a voltage-dependent block. Figure 4A shows the effect of DIDS on IMCD ClCa currents. DIDS, unlike NFA, blocks in a voltage-dependent manner. The outward current was blocked at positive voltages more than the inward currents at negative voltages. At 300 μM , DIDS blocked outward currents by 80.8% at $+100$ mV but inward currents by 54.9% at -100 mV (Fig. 4, D and E). The block was reversible. DPC behaved in a similar way. It also inhibited ClCa currents in a voltage-dependent manner (Fig. 4B). DPC (300 μM) blocked outward currents by 70.0% at $+100$ mV but inward currents by 44.4% at -100 mV (Fig. 4, D and E). The inhibition was also reversible. A9C reversibly blocked ClCa currents in a voltage-dependent manner (Fig. 4C). A9C (300 μM) blocked outward currents by 68.3% at $+100$ mV but inward currents only by 26.8% at -100 mV (Fig. 4, D and E).

DTT and tamoxifen. DTT, a reducing agent, has been reported to strongly block heterologously expressed CLCA currents (10, 14, 16). Figure 5A shows that 2 mM DTT has only a slightly inhibitory effect on outward ClCa currents in IMCD-K2 cells. The inhibition developed slowly. DTT (2 mM) inhibited the current by 35% at 100 mV in 4–6 min (Student's *t*-test, paired data, $P = 0.01$). A similar result was obtained in *X. laevis* oocytes (not shown).

Tamoxifen is an effective blocker for swelling-activated Cl^- channels (4) and CLCA (17), but it did not block ClCa currents after 3–6 min in either IMCD-K2 cells (Fig. 5B) or *X. laevis* oocytes (not shown).

DISCUSSION

Biophysical Properties of ClCa Currents in IMCD Cell Lines

ClCa currents have previously been studied in IMCD-3 and IMCD-K2 cell lines derived from IMCD.

ClCa currents in IMCD-3 cells (40) are different from those in IMCD-K2 cells. In the absence of any agents that would raise intracellular Ca^{2+} , the majority of IMCD-3 cells (64%) possessed a large, spontaneously active, outwardly rectifying, and time/voltage-independent Cl conductance (45). This suggested that the ClCa channels were open at resting Ca^{2+} levels. Changes in $[\text{Ca}^{2+}]_i$ produced by chelating cytosolic Ca^{2+} by preloading the cells with BAPTA-AM or by elevating cytosolic Ca^{2+} with ionomycin or ATP altered current

amplitude but did not alter the kinetics of the current (45). Because the biophysical properties are similar to those described for mouse CLCA1 functionally expressed in HEK-293 cells, it was suggested that the ClCa currents in IMCD-3 cells might be displayed by the CLCA family (10).

In contrast, ClCa currents in IMCD-K2 cells (27) showed time and voltage dependence. After the induction of slow ramps in $[\text{Ca}^{2+}]_i$ produced by exposing BAPTA-loaded IMCD-K2 cells to ionomycin, whole cell currents exhibited pronounced outward rectification with time-dependent activation or inactivation (3). We have extended these findings here. We applied whole cell recording to IMCD-K2 cells and observed the Ca^{2+} activation by directly changing $[\text{Ca}^{2+}]_i$. Lower Ca^{2+} (<800 nM) activated outwardly rectifying Cl^- currents, whereas high Ca^{2+} elicited nearly linear Cl^- currents. The currents activated at low Ca^{2+} showed time-dependent activation and deactivation. Ca^{2+} activation and Ca^{2+} affinity of the ClCa channel were voltage dependent. The Ca^{2+} activation of the channel was dose dependent, and the EC_{50} was $\sim 0.35 \mu\text{M}$ at +100 mV and $\sim 0.95 \mu\text{M}$ at -100 mV. These data indicate that ClCa currents in IMCD-K2 cells resemble those in secretory epithelia and *X. laevis* oocytes (2, 33).

One may be tempted to speculate that the differences in ClCa currents between IMCD-3 and IMCD-K2 cells may be related to the fact that IMCD-3 cells are derived from the terminal segment of the duct (40) and IMCD-K2 cells are derived from the initial segment (27). However, to our knowledge, there are no data on Ca^{2+} -activated Cl^- channels in intact IMCD. Therefore, one must consider the possibility that the ClCa currents in these cell lines may not reflect the situation in the intact tissue. To determine whether ClCa currents differ between initial and terminal segments of the IMCD, electrophysiological recording of native cells from different segments of IMCD may clarify this point.

Comparison of Properties of ClCa Currents Between *X. laevis* Oocytes and IMCD-K2 Cells

We have extensively studied ClCa channels in *X. laevis* oocytes (28, 38, 39). Comparing the properties of

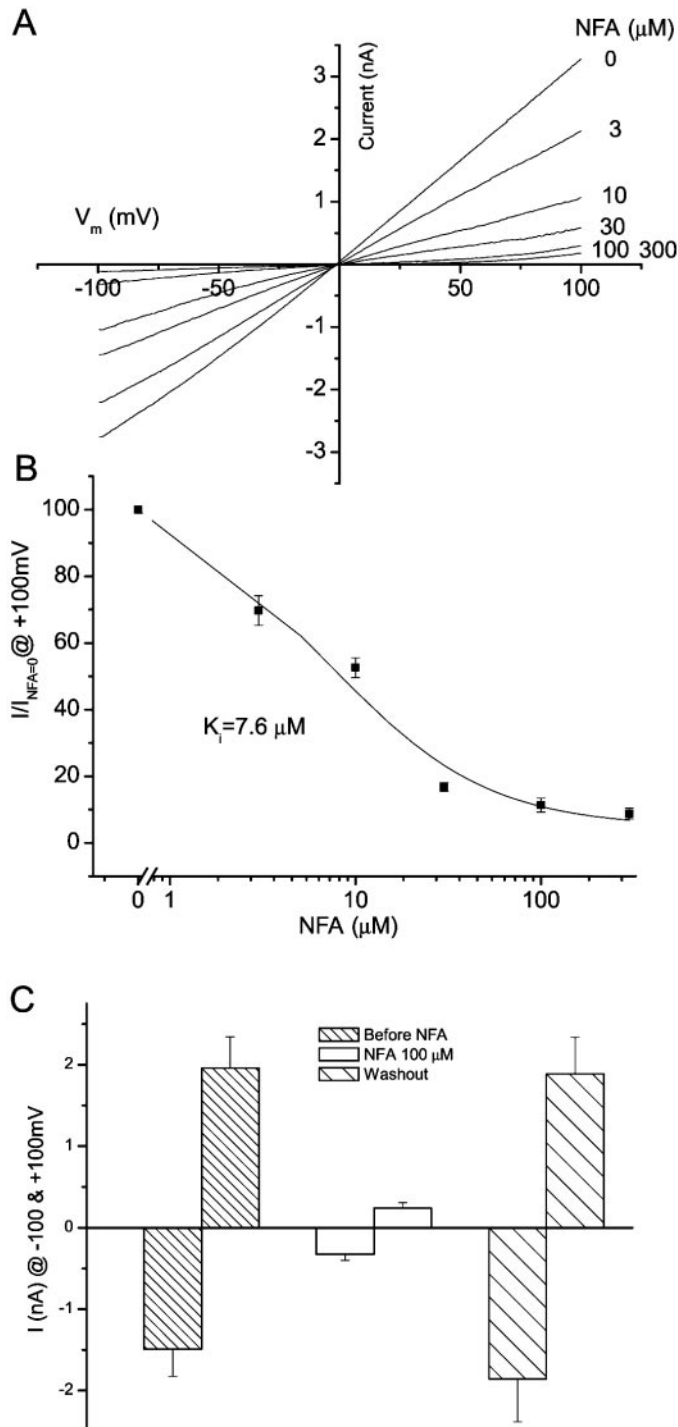


Fig. 3. Block of ClCa currents by external niflumic acid (NFA) in IMCD-K2 whole cell recordings. **A**: I - V relationships showing equal block of inward and outward ClCa currents by various NFA concentrations ($[\text{NFA}]$) in the bath. The whole cell patch was voltage clamped from the holding potential of -40 mV with a 200-ms-duration voltage ramp from -100 to +100 mV. Pipette solution contained high $[\text{Ca}^{2+}]_i$. The $[\text{NFA}]$ in the bath solution were 0, 3, 10, 30, and 100–300 μM . **B**: apparent K_i of NFA applied to the bath at V_m of +100 mV ($n = 5$). The data were fitted to the equation $I/I_{\text{NFA}=0} = I_{\text{min}} + (I_{\text{max}} - I_{\text{min}})/(1 + ([\text{NFA}]/K_i)^n)$, where I_{max} and I_{min} are the maximum and minimum current amplitudes, respectively, K_i is the concentration of NFA required to reduce the current amplitude to $(I_{\text{max}} + I_{\text{min}})/2$, and n is the slope factor. **C**: reversibility of block of ClCa currents by NFA in the bath. The patched cells were treated with 100 μM NFA in the bath, and then NFA was washed out. The currents at membrane potentials of -100 and +100 mV were measured and averaged ($n = 5$).

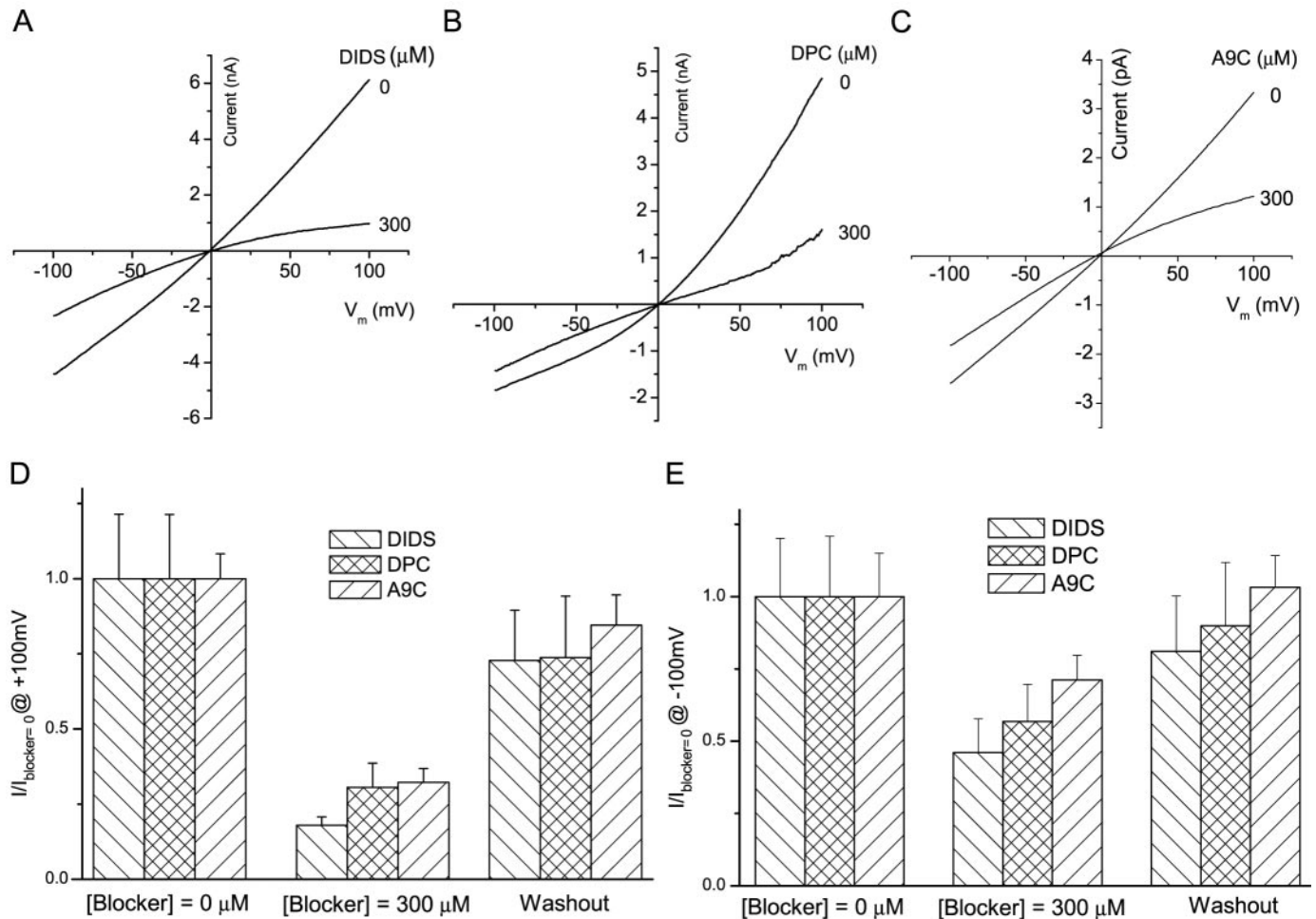


Fig. 4. A–C: I - V relationships of ClCa currents blocked by external DIDS, diphenylamine-2-carboxylic acid (DPC), and anthracene-9-carboxylic acid (A9C), respectively, in IMCD-K2 whole cell recordings. *D* and *E*: comparison of reversible block of outward (*D*) and inward (*E*) ClCa currents by blockers. DIDS (300 μM , $n = 5$), DPC ($n = 7$), or A9C ($n = 7$) was applied in the bath. For experimental conditions, refer to the legend to Fig. 3.

ClCa currents in oocytes with those in IMCD-K2 cells, we found that both channels resemble each other biophysically and pharmacologically, as summarized in Table 1. ClCa current activation in both cell types was controlled strictly by $[\text{Ca}^{2+}]_i$, and the Ca^{2+} activation showed voltage dependency. At low $[\text{Ca}^{2+}] < 1 \mu\text{M}$, the currents activated slowly on depolarization and deactivated on hyperpolarization and the steady-state I - V plot was strongly outwardly rectifying. At higher $[\text{Ca}^{2+}]$, the currents did not rectify and were time independent. This difference in behavior at different $[\text{Ca}^{2+}]$ was due to the different affinity of the channel for Ca^{2+} . Both ClCa channels showed a higher affinity for Ca^{2+} at positive V_m but a lower affinity at negative V_m . The affinity difference is about two- to threefold between -100 and $+100$ mV.

The similarity of the biophysical properties of ClCa channels for both IMCD-K2 and oocytes suggests a similar channel pore structure. The pharmacological properties support the hypothesis. We studied in detail the voltage-dependent block of ClCa channels by various anion blockers for Cl^- channels with excised

patches from oocytes. All drugs studied blocked the channel from the outside in a voltage-dependent manner. The order of block potency was $\text{NFA} > \text{A9C} > \text{DIDS} > \text{DPC}$ at $+100$ mV. Our analysis suggests that the channel is an elliptical cone with the largest opening facing the extracellular space (38). In this study, the four drugs applied in the bath also mainly blocked the outward ClCa currents in whole cell recordings of IMCD-K2 cells. The block also showed voltage dependence. The order of potency was similar to that for oocytes, although DIDS was more potent than A9C for IMCD-K2 cells (Table 1).

Molecular Identification of Potential Genes for ClCa Currents in IMCD-K2 Cells

So far, two molecular candidates for ClCa channels have been identified, bestrophins and CLCA. Bestrophin is the product of the gene isolated from a person with Best vitelliform macular dystrophy (VMD-2) by positional cloning (35, 37). Northern blot analysis has shown that bestrophin mRNA is strongly distributed in

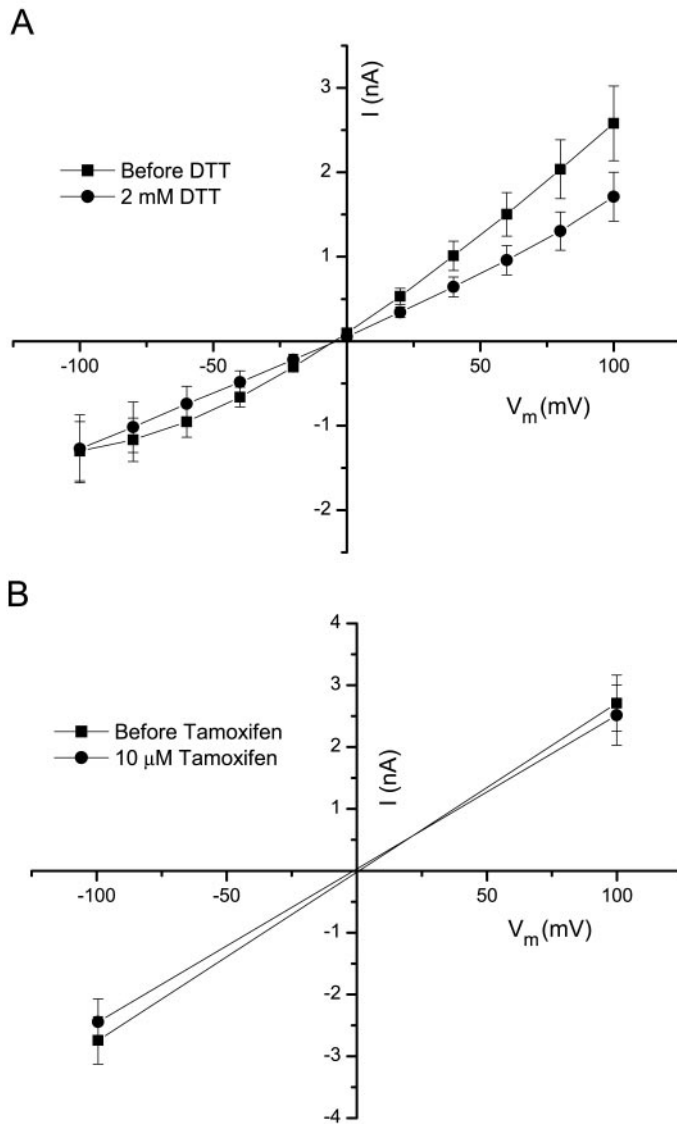


Fig. 5. *A*: effect of external DTT on ClCa currents in IMCD-K2 cells. Currents were recorded with step voltages. Voltage protocol refers to Fig. 1. The average currents ($n = 9$ for each) at the end of the 0.75-s pulse were plotted vs. membrane potentials. The patched cells were treated with 2 mM DTT for 4–6 min before being washed out. DTT inhibited outward ClCa currents in IMCD-K2 whole cell recordings. Difference significance was determined using Student's *t*-test (paired data, $P = 0.01$). *B*: no significant block of ClCa currents by external tamoxifen in IMCD-K2 whole cell recordings. Experimental conditions refer to the legend to Fig. 3. The currents at V_m of -100 and $+100$ mV were measured, averaged ($n = 5$), and plotted as *I*-*V* relationship.

retina, brain, and spinal cord, and RT-PCR has indicated that bestrophin also existed in kidney. Bestrophin localizes to the basolateral plasma membrane of the retinal pigment epithelium (RPE) (34) and contributes to the slow light peak of the electrooculogram (8). The function of bestrophins has been enigmatic until recently, Sun et al. (46) reported that human bestrophins are Ca^{2+} -sensitive Cl^- channels. Under whole cell recording, heterologously expressed human bestrophin-1 in HEK-293 cells showed voltage-independent Cl currents at 40 nM Ca^{2+} . The heterologously expressed human bestrophin-1 has very high sensitivity to Ca^{2+} . The EC_{50} is 0.1 μM at $+100$ mV, and the currents are time independent at all $[\text{Ca}^{2+}]$ (Qu Z, unpublished observations). These properties are different from those of ClCa currents in IMCD-K2 cells.

Although a putative family of Ca^{2+} -sensitive Cl channels (CLCA) has been cloned (1, 7, 10, 14–17, 43), this remains controversial. The properties of the heterologously expressed CLCA channels (10, 14, 15, 25) differ from those of native ClCa currents in various cells, but the possibility remains that a subunit is needed for CLCA channels to express currents like those for native ClCa. Mouse CLCA1 was cloned from a mouse lung library using homology cloning (10). The analysis of the tissue distribution of mCLCA1 showed strong expression in mouse epithelial tissues, including kidney. The properties of mouse CLCA1 have been studied by heterologous expression in HEK-293 cells (10). Mouse CLCA1 currents were activated by intracellular Ca^{2+} in whole cell recording. The currents were outwardly rectifying, but time independent at 2 μM $[\text{Ca}^{2+}]_i$. Obviously, the properties of mouse CLCA1 currents are not identical to those in IMCD-K2 cells.

Although our RT-PCR data indicated that the bestrophin and CLCA gene families were expressed in IMCD-K2 cells (data not shown), bestrophin and CLCA channels appear to be different from the ClCa currents we have studied in IMCD-K2 cells.

Physiological Functions of ClCa Conductance in IMCD-K2 Cells

Although the mouse and *X. laevis* are greatly separated from each other on the phylogenetic tree, the properties of ClCa channels in both species are very similar, indicating that the channel structure may be highly conserved; the IMCD-K2 cell line was originally established from the initial IMCD of mice (27). Reconstituted mouse IMCD-K2 epithelia electrogenically ab-

Table 1. Summary of comparison of ClCa currents in oocytes and IMCD-K2 cells

Cell Type	Ca^{2+} Activation	Voltage-Dependent Kinetics	Ca^{2+} EC_{50} , μM (-100 to $+100$ mV)	Hill Coefficient (-100 to $+100$ mV)	K_i NFA, μM	Pharmacology at $+100$ mV (Order of Potency)	Blocking Reversibility
<i>Xenopus laevis</i> oocytes	Direct	Yes	~ 1.6 to ~ 0.8	~ 3.0 to ~ 2.5	7.6	NFA > A9C > DIDS > DPC	DTT: slow inhibition; tamoxifen: no inhibition
IMCD-K2 cells	\pm	Yes	~ 0.95 to ~ 0.35	~ 3.0 to ~ 2.0	10.1	NFA > DIDS > DPC, A9C	DTT: slow inhibition; tamoxifen: no inhibition

ClCa, Ca^{2+} -activated Cl^- channel; IMCD, inner medullary collecting duct; NFA, niflumic acid; A9C, anthracene-9-carboxylic acid; DPC, diphenylamine-2-carboxylic acid; \pm , excised patch has not been done to prove this point.

sorb Na^+ (12, 27) through nucleotide-gated cation channels and display transepithelial anion secretion (27). Anion secretion in IMCD-K2 cells involves uphill accumulation of $\text{Cl}^-/\text{HCO}_3^-$ across the basolateral membrane, followed by downhill movement across the apical membrane through Cl^- channels. Boese et al. (3) presented evidence that ClCa conductance was present at the apical membrane of reconstituted IMCD-K2 epithelial layers and participated in transepithelial anion secretion when ATP and ionomycin were applied to the layers. It is likely that a variety of hormones and paracrines can activate apical ClCa currents and affect IMCD anion secretion via increasing $[\text{Ca}^{2+}]_i$.

Wild-type CFTR was also expressed in all segments of rat kidney nephron, including IMCD (36). Cl^- currents mediated by CFTR were also revealed in IMCD and IMCD-K2 cells (3, 22, 48). Because the renal deficit in cystic fibrosis is not profound compared with that in the pancreas or small intestine, alternative mechanisms must exist to compensate for the loss of CFTR function (11, 44, 49). The possibility exists that ClCa in mouse IMCD may compensate for defective CFTR. It has been hypothesized that the severity of the deficit due to defective CFTR in different organs correlates with the expression of an apical-epithelial ClCa conductance and that this ClCa conductance can functionally compensate for the loss of CFTR activity in humans as in the transgenic cystic fibrosis mouse (5, 11, 49).

DISCLOSURES

This study was supported by National Institute of General Medical Sciences Grant GM-60448 (to H. C. Hartzell) and a fellowship from the American Heart Association (to Z. Qu).

REFERENCES

1. Agnel M, Verinat T, and Culouscou JM. Identification of three novel members of the calcium-dependent chloride channel (CaCC) family predominantly expressed in the digestive tract and trachea. *FEBS Lett* 455: 295–301, 1999.
2. Begenisich T and Melvin JE. Regulation of chloride channels in secretory epithelia. *J Membr Biol* 163: 77–85, 1998.
3. Boese SH, Glanville M, Aziz O, Gray MA, and Simmons NL. Ca^{2+} and cAMP-activated Cl^- conductances mediate Cl^- secretion in a mouse renal inner medullary collecting duct cell line. *J Physiol* 523: 325–338, 2000.
4. Boese SH, Glanville M, Gray MA, and Simmons NL. The swelling-activated anion conductance in the mouse renal inner medullary collecting duct cell line mIMCD-K2. *J Membr Biol* 177: 51–64, 2000.
5. Clarke LL, Grubb BR, Yankaskas JR, Cotton CU, McKenzie A, and Boucher RC. Relationship of a non-cystic fibrosis transmembrane conductance regulator-mediated chloride conductance to organ-level disease in *Cftr*^{-/-} mice. *Proc Natl Acad Sci USA* 91: 479–483, 1994.
6. Collier ML, Levesque PC, Kenyon JL, and Hume JR. Unitary Cl^- channels activated by cytoplasmic Ca^{2+} in canine ventricular myocytes. *Circ Res* 78: 936–944, 1996.
7. Cunningham SA, Awayda MS, Bubien JK, Ismailov II, Arrate MP, Berdiev BK, Benos DJ, and Fuller CM. Cloning of an epithelial chloride channel from bovine trachea. *J Biol Chem* 270: 31016–31026, 1995.
8. Francois J, De Rouck A, and Fernandez-Sasso D. Electrophysiology in vitelliform degeneration of the macula. *Arch Ophthalmol* 77: 726–733, 1967.
9. Frings S, Reuter D, and Kleene SJ. Neuronal Ca^{2+} -activated Cl^- channels—homing in on an elusive channel species. *Prog Neurobiol* 60: 247–289, 2000.
10. Gandhi R, Elble RC, Gruber AD, Schreur KD, Ji HL, Fuller CM, and Pauli BU. Molecular and functional characterization of a calcium-sensitive chloride channel from mouse lung. *J Biol Chem* 273: 32096–32101, 1998.
11. Gray MA, Winpenny JP, Porteous DJ, Dorin JR, and Argent BE. CFTR and calcium-activated chloride currents in pancreatic duct cells of a transgenic CF mouse. *Am J Physiol Cell Physiol* 266: C213–C221, 1994.
12. Green RB, Slattery MJ, Gianferrari E, Kizer NL, McCoy DE, and Stanton BA. Hyperosmolality inhibits sodium absorption and chloride secretion in mIMCD-K2 cells. *Am J Physiol Renal Fluid Electrolyte Physiol* 271: F1248–F1254, 1996.
13. Greger R. The membrane transporters regulating epithelial NaCl secretion. *Pflügers Arch* 432: 579–588, 1996.
14. Gruber AD, Elble RC, Ji HL, Schreur KD, Fuller CM, and Pauli BU. Genomic cloning, molecular characterization, and functional analysis of human CLCA1 , the first human member of the family of Ca^{2+} -activated Cl^- channel proteins. *Genomics* 54: 200–214, 1998.
15. Gruber AD, Gandhi R, and Pauli BU. The murine calcium-sensitive chloride channel (mCaCC) is widely expressed in secretory epithelia and in other select tissues. *Histochem Cell Biol* 110: 43–49, 1998.
16. Gruber AD and Pauli BU. Molecular cloning and biochemical characterization of a truncated, secreted member of the human family of Ca^{2+} -activated Cl^- channels. *Biochim Biophys Acta* 1444: 418–423, 1999.
17. Gruber AD, Schreur KD, Ji HL, Fuller CM, and Pauli BU. Molecular cloning and transmembrane structure of hCLCA2 from human lung, trachea, and mammary gland. *Am J Physiol Cell Physiol* 276: C1261–C1270, 1999.
18. Hartzell HC, Machaca K, and Hirayama Y. Effects of adenosine-3',5'-bisphosphate and inositol-1,4,5-trisphosphate on Cl^- currents in *Xenopus laevis* oocytes. *Mol Pharmacol* 51: 683–692, 1997.
19. Hirakawa Y, Gericke M, Cohen RA, and Bolotina VM. Ca^{2+} -dependent Cl^- channels in mouse and rabbit aortic smooth muscle cells: regulation by intracellular Ca^{2+} and NO. *Am J Physiol Heart Circ Physiol* 277: H1732–H1744, 1999.
20. Husted RF and Stokes JB. Separate regulation of Na^+ and anion transport by IMCD: location, aldosterone, hypertonicity, TGF- β 1, and cAMP. *Am J Physiol Renal Fluid Electrolyte Physiol* 271: F433–F439, 1996.
21. Husted RF, Volk KA, Sigmund RD, and Stokes JB. Anion secretion by the inner medullary collecting duct. Evidence for involvement of the cystic fibrosis transmembrane conductance regulator. *J Clin Invest* 95: 644–650, 1995.
22. Husted RF, Zhang C, and Stokes JB. Concerted actions of IL-1 β inhibit Na^+ absorption and stimulate anion secretion by IMCD cells. *Am J Physiol Renal Fluid Electrolyte Physiol* 275: F946–F954, 1998.
23. Jaffe LA and Cross NL. Electrical regulation of sperm-egg fusion. *Annu Rev Physiol* 48: 191–200, 1986.
24. Jentsch TJ, Stein V, Weinreich F, and Zdebik AA. Molecular structure and physiological function of chloride channels. *Physiol Rev* 82: 503–568, 2002.
25. Ji HL, DuVall MD, Patton HK, Satterfield CL, Fuller CM, and Benos DJ. Functional expression of a truncated Ca^{2+} -activated Cl^- channel and activation by phorbol ester. *Am J Physiol Cell Physiol* 274: C455–C464, 1998.
26. Kidd JF and Thorn P. Intracellular Ca^{2+} and Cl^- channel activation in secretory cells. *Annu Rev Physiol* 62: 493–513, 2000.
27. Kizer NL, Lewis B, and Stanton BA. Electrogenic sodium absorption and chloride secretion by an inner medullary collecting duct cell line (mIMCD-K2). *Am J Physiol Renal Fluid Electrolyte Physiol* 268: F347–F355, 1995.
28. Kuruma A and Hartzell HC. Bimodal control of a Ca^{2+} -activated Cl^- channel by different Ca^{2+} signals. *J Gen Physiol* 115: 59–80, 2000.
29. Kuruma A and Hartzell HC. Dynamics of calcium regulation of chloride currents in *Xenopus* oocytes. *Am J Physiol Cell Physiol* 276: C161–C175, 1999.

30. **Large WA and Wang Q.** Characteristics and physiological role of the Ca^{2+} -activated Cl^- conductance in smooth muscle. *Am J Physiol Cell Physiol* 271: C435–C454, 1996.
31. **Machaca K and Hartzell HC.** Reversible Ca gradients between the subplasmalemma and cytosol differentially activate Ca-dependent Cl currents. *J Gen Physiol* 113: 249–266, 1999.
32. **Machaca K and Hartzell HC.** Asymmetrical distribution of Ca-activated Cl channels in *Xenopus* oocytes. *Biophys J* 74: 1286–1295, 1998. [Corrigenda. *Biophys J* 74 June 1998, p. 3313.]
33. **Machaca K, Qu Z, Kuruma A, Hartzell HC, and McCarty N.** The endogenous Ca^{2+} -activated Cl channel in *Xenopus* oocytes: a physiologically and biophysically rich model system. In: *Current Topics in Membranes*, edited by Fuller CM. New York: Elsevier, 2002, vol. 53, p. 3–39.
34. **Marmorstein AD, Marmorstein LY, Rayborn M, Wang X, Hollyfield JG, and Petrukhin K.** Bestrophin, the product of the Best vitelliform macular dystrophy gene (VMD2), localizes to the basolateral plasma membrane of the retinal pigment epithelium. *Proc Natl Acad Sci USA* 97: 12758–12763, 2000.
35. **Marquardt A, Stohr H, Passmore LA, Kramer F, Rivera A, and Weber BH.** Mutations in a novel gene, VMD2, encoding a protein of unknown properties cause juvenile-onset vitelliform macular dystrophy (Best's disease). *Hum Mol Genet* 7: 1517–1525, 1998.
36. **Morales MM, Carroll TP, Morita T, Schwiebert EM, Devuyt O, Wilson PD, Lopes AG, Stanton BA, Dietz HC, Cutting GR, and Guggino WB.** Both the wild type and a functional isoform of CFTR are expressed in kidney. *Am J Physiol Renal Fluid Electrolyte Physiol* 270: F1038–F1048, 1996.
37. **Petrukhin K, Koisti MJ, Bakall B, Li W, Xie G, Marknell T, Sandgren O, Forsman K, Holmgren G, Andreasson S, Vujic M, Bergen AA, McGarty-Dugan V, Figueroa D, Austin CP, Metzker ML, Caskey CT, and Wadelius C.** Identification of the gene responsible for Best macular dystrophy. *Nat Genet* 19: 241–247, 1998.
38. **Qu Z and Hartzell HC.** Functional geometry of the permeation pathway of Ca^{2+} -activated Cl^- channels inferred from analysis of voltage-dependent block. *J Biol Chem* 276: 18423–18429, 2001.
39. **Qu Z and Hartzell HC.** Anion permeation in Ca^{2+} -activated Cl^- channels. *J Gen Physiol* 116: 825–844, 2000.
40. **Rauchman MI, Nigam SK, Delpire E, and Gullans SR.** An osmotically tolerant inner medullary collecting duct cell line from an SV40 transgenic mouse. *Am J Physiol Renal Fluid Electrolyte Physiol* 265: F416–F424, 1993.
41. **Rocha AS and Kudo LH.** Factors governing sodium and chloride transport across the inner medullary collecting duct. *Kidney Int* 38: 654–667, 1990.
42. **Rocha AS and Kudo LH.** Atrial peptide and cGMP effects on NaCl transport in inner medullary collecting duct. *Am J Physiol Renal Fluid Electrolyte Physiol* 259: F258–F268, 1990.
43. **Romio L, Musante L, Cinti R, Seri M, Moran O, Zegarra-Moran O, and Galietta LJ.** Characterization of a murine gene homologous to the bovine CaCC chloride channel. *Gene* 228: 181–188, 1999.
44. **Simmons NL.** Renal epithelial Cl^- secretion. *Exp Physiol* 78: 117–137, 1993.
45. **Stewart GS, Glanville M, Aziz O, Simmons NL, and Gray MA.** Regulation of an outwardly rectifying chloride conductance in renal epithelial cells by external and internal calcium. *J Membr Biol* 180: 49–64, 2001.
46. **Sun H, Tsunenari T, Yau KW, and Nathans J.** The vitelliform macular dystrophy protein defines a new family of chloride channels. *Proc Natl Acad Sci USA* 99: 4008–4013, 2002.
47. **Tsien RY and Pozzan T.** Measurements of cytosolic free Ca^{2+} with Quin-2. *Methods Enzymol* 172: 230–262, 1998.
48. **Vandorpe D, Kizer N, Ciampollilo F, Moyer B, Karlson K, Guggino WB, and Stanton BA.** CFTR mediates electrogenic chloride secretion in mouse inner medullary collecting duct (mIMCD-K2) cells. *Am J Physiol Cell Physiol* 269: C683–C689, 1995.
49. **Winpenny JP, Verdon B, McAlroy HL, Colledge WH, Ratcliff R, Evans MJ, Gray MA, and Argent BE.** Calcium-activated chloride conductance is not increased in pancreatic duct cells of CF mice. *Pflügers Arch* 430: 26–33, 1995.
50. **Zeidel ML.** Hormonal regulation of inner medullary collecting duct sodium transport. *Am J Physiol Renal Fluid Electrolyte Physiol* 265: F159–F173, 1993.